Spectral investigation of Mercury's pits' surroundings: Constraints on the planet's explosive activity

Océane Barraud, Sébastien Besse, Alain Doressoundiram, Thomas Cornet, Claudio Muñoz

Spectral investigation of Mercury's pits' surroundings: Constraints on the planet's explosive activity

Authors: Océane Barraud[1] (corresponding author), Sébastien Besse[2], Alain Doressoundiram[1], Thomas Cornet[2] and Claudio Munoz[2].

Affiliations:
[1]LESIA, Observatoire de Paris, Université PSL, CNRS, Sorbonne Université, Université de Paris, 5 place Jules Janssen, 92195 Meudon, France.
[2]Aurora Technology B.V., European Space Astronomy Centre/ESA, Madrid, Spain.

Abstract. The understanding of volcanic explosive episodes on the surface of Mercury has important implications for the origin, history and inventory of Mercury's volatiles and for the thermal evolution of the planet. The hermean explosive features are pits, interpreted as endogenic pyroclastic vents often surrounded by bright and diffuse deposits, named faculae, and interpreted as pyroclastic material. We present a global spectroscopic survey of the surroundings of the listed endogenous pits, derived from spectra obtained by the Mercury Atmospheric and Surface Composition Spectrometer (MASCS/MESSENGER). The spectral properties of 26 faculae around endogenous pits were characterized. The diameter of 80% of them has been reassessed upwards by 17 km on average, implying volatile contents needed to emplace these deposits consequently higher than estimated in previous studies. These observations suggest a higher bulk volatile content or subsurface volatile enhancement. Spectral similarities between faculae located in the same crater indicate either a similar magmatic source or a large fraction of country rocks. The size, volatile content, location, and spectral properties of Nathair Facula seem to indicate an anomaly with respect to the other faculae that may be explained by a phreatomagmatic-like event by interaction between hot-magma and local carbon-rich layer.

1. Introduction

The remains of the hermean explosive activity were first observed by the MErcury Surface, Space ENvironment, GEochemistry, and Ranging (MESSENGER) spacecraft on the edge of the Caloris basin (Head et al., 2008). Subsequently, additional potential features were identified on impact crater floors and on smooth plains elsewhere (Kerber et al., 2009, Kerber et al., 2011). The explosive features are represented on Mercury by pits and faculae. Pits are interpreted to be endogenic pyroclastic vents on the basis of their irregular and often elongated morphology and their lack of associated raised rim (Pegg et al., 2021). Referred first as red-spots, faculae are high-albedo (compared to Mercury's average), spectrally red (increasing reflectance with increasing wavelength), and surficial deposits that have diffuse margins. Faculae with central pits are interpreted as pyroclastic deposits formed by the fragmentation and ejection of magma particles driven by volatile species released from rising magma (Wilson and Head, 1981). Therefore, such faculae represent important sources of information about planetary physical and geochemical properties, including thermal history, interior structure and volatile budgets.

Since the first flyby of MESSENGER, several global mappings of explosive volcanic features, based on images from the Mercury Dual Imaging System (MDIS) have been done (Kerber et al., 2009, Kerber et al., 2011, Goudge et al., 2014, Jozwiak et al., 2018). The first catalogues were based on the concomitance between pits and the surrounding faculae. Thomas et al., (2014b) used a different approach by inventorying hermean endogenous pits even if they were not surrounded by faculae. They listed, first, 327 pits regrouped in 174 candidate endogenic pit sites,

150 of which possess a red spectral anomaly and high albedo in their surroundings. This number was reassessed to 353 pits in 184 pit sites by Thomas (2015). Around 79 % of pits surrounded by facula occur within an impact crater (Thomas et al., 2014b). This correlation may be the result of the easier ascent of the magma because of impact-induced fracturation and crustal weaknesses beneath the largest impact features (e.g., Klimczak et al., 2018). Stratigraphic relationships, degradation state of the host impact craters and the datation of certain faculae suggest that the explosive volcanic activity on Mercury likely occurred over a substantial fraction of Mercury's geologic history, with the emplacement of some pyroclastic deposits from at least 3.9 Ga until less than a billion years ago (Goudge et al., 2014; Thomas et al., 2014a).

Compositional information, derived from visible to near-infrared spectroscopic observations, as well as X-ray, neutron, and gamma-ray spectrometry, can be used to characterize the explosive activity of the planet as well as to make inferences about the nature and origin of the pyroclasts constituting the faculae. Spectral investigations of the faculae with the Mercury Atmospheric and Surface Composition spectrometer (MASCS) revealed, in addition to a red slope in the visible and high reflectance at 750 nm, a strong downturn of the reflectance in the ultraviolet (Goudge et al., 2014). Besse et al., (2015) investigated spectral properties of the faculae and demonstrated that, as on the Moon (Jawin et al. 2015), they change as a function of distance to the central vent. Besse et al., (2020) used these spectral variations to define the extent of 14 faculae at the surface of Mercury by using for each deposit the 3 best orbits of MASCS. They reassessed the radius of 65 % of the faculae analyzed upwards, and demonstrated the implications of these results on the volatile contents needed to drive explosive eruptions on Mercury.

Here we investigate the spectral properties of the surroundings of the endogenous pits listed by Thomas et al (2014b) and Thomas et al., (2015) with MASCS in order to extend the analysis done by Besse et al, (2020). All the MASCS available observations are used with the aim to better constrain the size and shape of the faculae. The spectral properties of the faculae are then analyzed and discussed to understand their composition and origin.

2. Search for spectral anomaly in the Mercury's pits' surroundings

The Visible and Infrared Spectrograph (VIRS) of the Mercury Atmospheric and Surface Composition Spectrometer (MASCS) instrument is a non-imaging point spectrometer operating between 300 and 1450 nm (McClintock & Lankton, 2007) with a spectral resolution of 5 nm. A visible (VIS) detector is sensitive to wavelengths that extend from 300 to 900 nm, and a near-infrared (NIR) detector to wavelengths between 900 to 1450 nm (McClintock & Lankton, 2007).
In this study, we used the VIRS Derived Data Record (DDR) data products available on the Planetary Data System (PDS). These data have been radiometrically and photometrically calibrated by the MESSENGER team. Additional processing, using the method developed by Besse et al., (2015), is applied to the data to combine the VIS and NIR data in a continuous spectrum from 300 to 1450 nm. A first step consists in removing the outliers deviating by more than 2 sigma. Only the most distant outliers are removed using this method, which represents less than 1% of the measurements by the VIS detector and less than 4% in the NIR (Barraud et al., 2020). In a second step, a moving average window of 3 points is applied to the entire VIS and NIR, reducing the scatter of the channel-to-channel reflectance. Finally, an offset is applied to the NIR to combine the two parts of the spectrum (Besse et al., 2015). The approach tested on lunar spectra by Besse et al. (2015) has been validated for observations of Mercury's surface.

2.1. Data selection and significance level

The average diameter of the faculae measured by Kerber et al., (2011) is 46 km and by Besse et al., (2020) is 64 km. Thus, the MASCS/VIRS spectra are selected in a 100x100 km area around each pit (Thomas et al., 2014b, Jozwiak et al., 2018). The dimension of the area is then adjusted if necessary. For example, the area around the pit centered (35.8°N, 63.8°E) in Nathair Facula (Rothery et al., 2021) is enlarged to a 400 km square to include the entire facula which is interpreted as the largest pyroclastic deposit on Mercury. The selection box is conversely reduced if the deposit radius is known to be smaller to optimise the computing time.

The selected observations are then filtered by instrument temperature and incidence angle. The NIR detector is more susceptible to increased background and noise from high temperatures (Izenberg et al., 2014). However, the effect of high temperature on MASCS/VIRS spectra is not fully characterized at this stage. Therefore, the data recorded in the highest temperature regime of the instrument (temperature exceeding 40°C) are discarded. High phase angles affect the detected spectral reflectance, which is more sensitive to local topography. In order to secure the comparison between faculae at different geographical locations, observations made at incidence angles greater than 75° have also been removed.

In each of the selected areas around the pits, a significance level (**Table 1**) for the analysis of spectral anomalies is established based on:

- The number of observations. First quality index Q_1 is the ratio between the number of footprints in the region and the number of footprints with the median spatial resolution of MASCS at the planet scale needed to cover the selected region. The median spatial resolution of the MASCS footprints is calculated from 3,677,857 filtered (temperature and incidence angle) observations and corresponds to 6 km². As an example, for a Q_1 equal to 100 % in an area of 10 000 km², the ideal number of evenly spaced footprints should be 1667.
- The spatial coverage of MASCS footprints. A second quality index Q_2 corresponds to the ratio between the total coverage of the footprints in the region to the area of the region.
- The spatial distribution of observations around the pit. The third and fourth quality index Q_3 and Q_4 evaluate the distribution of footprints respectively by concentric 10 km-wide rings and by 90° azimuth intervals around the vent (**Figure 1**).

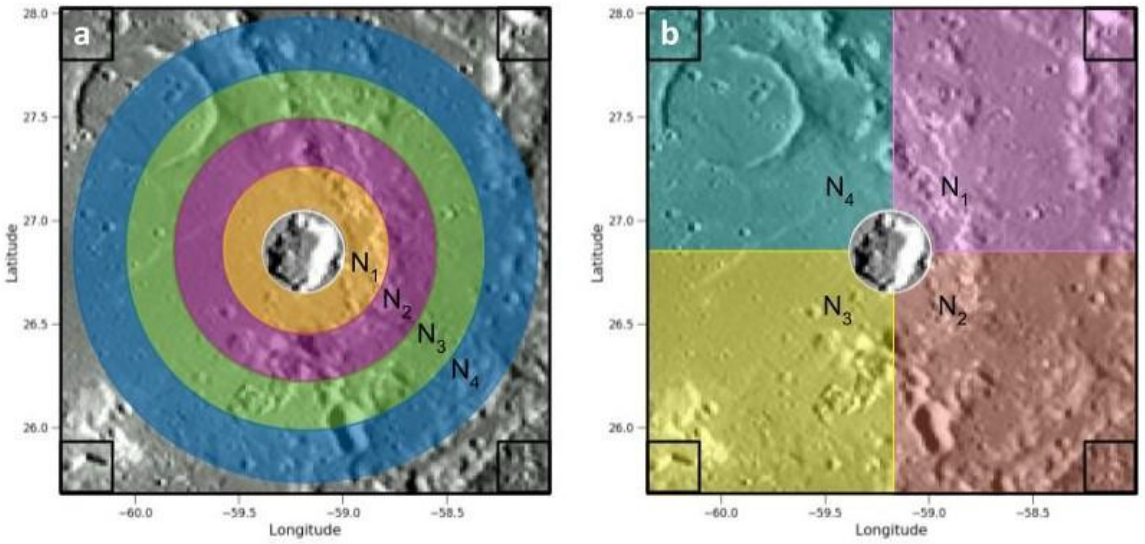

Figure 1: *Area (100 km square) selected around a pit in Praxiteles impact crater (26.85°N; 59.18°W). The pit is surrounded by a white circle. a) Distribution of the 10 km intervals around the pit. The number of intervals depends on the size of the selected area. b) Distribution of the 90° azimuth intervals around the pit. N_i is the number of observations in the colored region (**Table 1**). The black squares at the corners indicate the region used to define the local spectral properties of the background.*

Depending on the values of the previously defined quality indexes (**Table 1**), the significance level (SL) is represented by a score between 1 and 5. Since its individual score can reach 2 (see **Table 1**), Q1 has more importance than the other quality indexes. If the SL is between 0 and 2, spectral analysis cannot be done with MASCS observations. If the SL is 3, spectral analysis can be done but the result must be treated with caution and validated visually. If the SL is equal to 4 or 5, the total number and spatial distribution of the observations ensure the proper analysis of a spectral anomaly. Given its spatial coverage and its average spatial resolution, a spectral anomaly in an area below 500 km² (10-12 km radius area) is difficult to properly analyze with MASCS (value arbitrarily defined).

Table 1: *Definition of quality indexes and significance level.* A *corresponds to the area of the region (km²).* N_A *is the number of observations in the selected area.* $A_{footprints}$ *is the sum of the area covered by the footprints.* N_i *is the number of observations in the region i of the selected area (**Figure 1**).*

Quality index	Mathematical formula	Values	Equivalence in significance level
Q_1	$Q_1 = \frac{N_A}{A/6}$	$Q_1 < 0.15$ $0.15 \leq Q_1 < 0.45$ $0.45 \leq Q_1$	0 1 2
Q_2	$Q_2 = \frac{A_{footprints}}{A}$	$Q_2 < 0.25$ $Q_2 \geq 0.25$	0 1
Q_3	$Q_3 = 1 - median\left[\left\lvert\frac{N_i - N_{i+1}}{N_i + N_{i+1}}\right\rvert, \left\lvert\frac{N_{i+1} - N_{i+2}}{N_{i+1} + N_{i+2}}\right\rvert, \ldots\right]$ (**Fig. 1a**)	$Q_3 < 0.5$ $Q_3 \geq 0.5$	0 1
Q_4	$Q_4 = 1 - median\left[\left\lvert\frac{N_1 - N_2}{N_1 + N_2}\right\rvert, \left\lvert\frac{N_2 - N_3}{N_2 + N_3}\right\rvert, \left\lvert\frac{N_3 - N_4}{N_3 + N_4}\right\rvert, \left\lvert\frac{N_4 - N_1}{N_4 + N_1}\right\rvert\right]$ (**Fig. 1b**)	$Q_4 < 0.5$ $Q_4 \geq 0.5$	0 1
Significance level			5/5

2.2. Spectral analysis

Based on previous studies (Goudge et al., 2014, Besse et al., 2015, Besse et al., 2020), the slope in the visible (VIS), the downturn of reflectance in the ultraviolet (UV) and the absolute reflectance in the visible seem the best indicators for the presence of faculae. The spectral parameters used are summarized in **Table 2**. The absolute reflectance at 750 nm (R750) and at 575 nm (R575) are average values of 3 points due to the smoothing of the data (Besse et al., 2015). The slope parameters are normalized to the reference spectrum provided by Izenberg et al. (2014), who computed it from the average of 850,000 spectra of Mercury's surface. By definition, slopes are equal to 1 for the average surface of Mercury.

The spectral properties of pyroclastic deposits are known to change as a function of distance from their source on Mercury (Besse et al., 2015, Besse et al., 2020). Therefore, to identify possible faculae around the pit, the spectral parameters are investigated in the selected area as a function of distance to the central pit. Some pits are located in terrains presenting spectral properties that differ from Mercury's mean surface. This is the case for pits located in the Caloris basin, which is spectrally different from Mercury's background (Head et al., 2009). In order to eliminate the possible contribution of the background terrain, which could hinder the characterisation of the faculae, the spectral parameters are normalized by a local average. Observations located in 10 by 10 km squares at each corner of the selected area are used to define the local average (**Fig. 1**). On the generic assumption that the faculae are mostly circular and centered on the pits, these regions are considered to be representative of the background material and free of pyroclastic material. If a corner area falls in a closed pit/faculae (as for the SW corner in **Fig. 1**), the observations are removed in this area. A faculae is recognized when at least the spectral parameters UV-downturn, VIS-slope and R750 are greater than the local mean close to the pit and decrease from the pit to a certain distance, interpreted as the limit of the facula, where they reach the local average.

Table 2: *Mathematical formulas of spectral parameters used to detect and analyze the spectral anomalies linked to faculae.* R_λ *is the absolute reflectance at the wavelength λ.*

Parameter	Spectral range (nm)	Mathematical definition
UV-downturn (Goudge et al., 2014)	300-400	$Depth_{303} + Depth_{324} + Depth_{350}$ where, $Depth_\lambda = \left[R_{401} - (401 - \lambda)\frac{R_{750} - R_{445}}{750-445}\right]/R_\lambda$
R575	570-580	R_{575}
R750	745-755	R_{750}
VIS-slope (S_{vis})	445-750	$R_\lambda = S_{vis} \times \lambda + b$

2.3. Global investigation

Global investigations of Mercury's pit surroundings reveal that 73 pit sites (with a total of 146 individual pits) were not sufficiently observed with MASCS to be analyzed in this study. This result is mainly due to the spatial coverage of the spectrometer. 88 pits lack data within a 10 km distance from the pit and the 58 other pits have a significance level lower or equal 2. 38 % (56) of the pits insufficiently observed with MASCS are located in the southern hemisphere compared to 61 % (215) for all pits (**Figure 2**). This result therefore confirms that the main factor limiting the study of pit surroundings is the spatial coverage which is lower in the northern hemisphere because of MESSENGER's highly eccentric orbit (Solomon et al., 2007). In addition, 77 pit sites (118 individual pits) do not display a spectral anomaly despite their good significance level (greater or equal to 3).

The 34 remaining pit sites (89 individual pits) display a spectral anomaly in near-ultraviolet to visible domains (**Figure 2**). We focused our analysis on these pits, in order to better understand the pyroclastic activity of Mercury. Among these pits, 61 (69 %) are in the southern hemisphere.

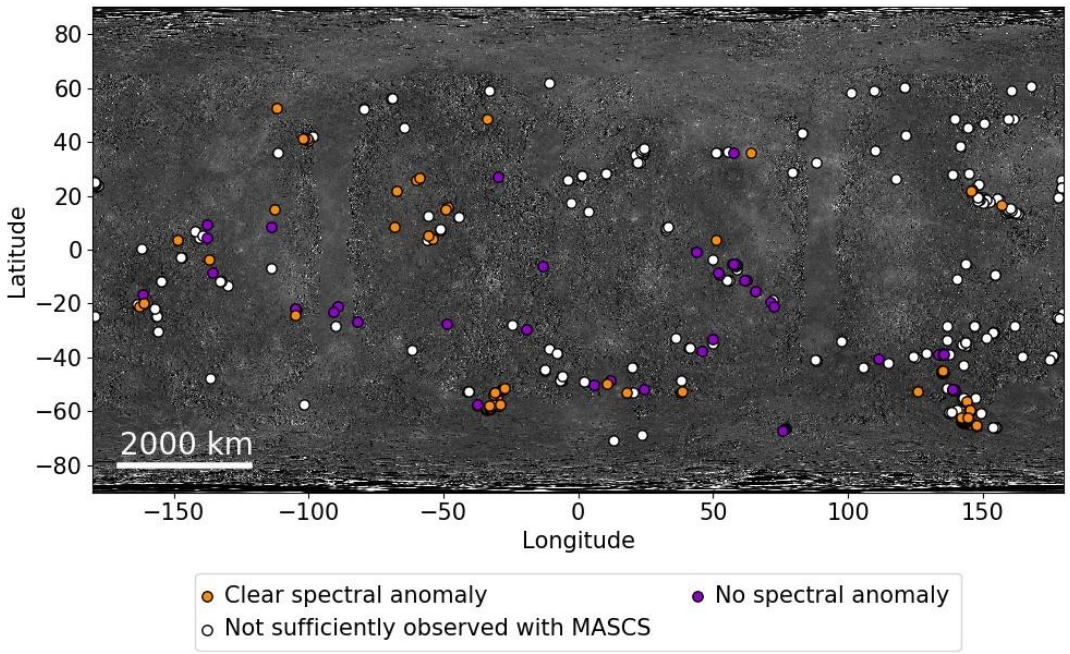

Figure 2: *Distribution of pits at the surface of Mercury. The pits' geographic locations are from Thomas et al. (2014b) and Jozwiak et al., (2018). The background map is the Basemap Reduced Data Record (BDR) from Mercury Dual Imaging System (32 pixels/degree, Denevi et al., 2018).*

3. Analysis of faculae

The analysis of the faculae around the pits is done under the assumption that on an airless body, such as Mercury, the final shape of pyroclastic deposits is mostly circular and centred on the volcanic vent. In the case where the volcanic vent is considered as a single pit, it is relatively simple to determine the radius of the facula using the method developed by Besse et al. (2020). However, the proximity of some pits, involving an overlap of circular deposits, complicates their individual spectral analysis. Several assumptions are therefore taken into account depending on the proximity and arrangement of the pits within a pit site:

- When a pit site contains multiple pits close to each other, the pits were counted as a multiple/compound volcanic vent. The centre was defined to be in the centre of the pit site and the radius of the volcanic vent to encompass all the pits (**Fig. S1a**).
- When the pits in a single pit site were sufficiently far apart from each other, they were considered as separate volcanic vents. This is for example the case for the pit site numbered 1047 by Thomas et al. (2020) in Praxiteles impact crater. The 3 pits identified are considered as 2 volcanic vents (1 simple vent and 1 compound vent) separated by 60 km (**Fig. S1a**). The pits from these two first categories are listed in **Table 3**.
- When the pits of a pit site were not close enough to be considered as a unique volcanic vent but too close to be considered as separate vents, and when the pits could not be approximated by circles (**Fig. S1b**), the dimensions of the faculae could not be estimated. These pits are listed in **Table S1** and need further individual study. They will not be mentioned in the rest of this study.

3.1. Extent of faculae

3.1.1. Nathair and Orm Faculae

Nathair Facula, which is the largest known facula on Mercury, and possibly in the inner Solar System, has been analyzed in detail by Thomas et al. (2014b), Besse et al., (2020) and Rothery et al., (2021). Its radius is well constrained to about 140 km. In their study, Besse et al. (2020) used 3 MASCS orbits which represent 604 footprints in this region, to characterize the extent of this facula. Here, Nathair Facula is investigated with 9917 footprints (44 orbits). While the parameters are normalized by Mercury's mean spectrum in the analysis of Besse et al., (2020), here they are normalized by the local mean. As in Besse et al., (2020), the linear decay of the spectral parameters from the volcanic vent to the edge of the deposit is used to define the radius of the deposit. A linear fit is adjusted to the normalized parameters VIS-slope, UV-downturn, R575 and R750. The radius is defined as the distance to the vent where the linear fit reaches the value of the local average (1 for the normalized parameters). Given the spatial resolution of MASCS and the diffuse character of faculae borders, the radius is estimated with an uncertainty of ± 5 km. In line with previous studies, the radius of Nathair Facula is estimated at 140 ± 5 km validating this mathematical approach (**Fig. 3**). Also, the radius of Orm Faculae (SW vent) in Praxiteles impact crater defined by Besse et al. (2020) to 28 km is confirmed as 30 ± 5 km (**Fig. 4**). Using this method, 26 faculae have been measured around the volcanic pits listed in **Table 3**.

Interestingly, Rothery et al., (2021) demonstrated that the Nathair facula's midpoint is offset by 10–30 km northwards or northeastwards from the volcanic vent. This asymmetry is confirmed with the larger amount of data used here. Observations with an azimuth around 180° (south of the facula) lie below the linear regression line comprising all azimuths while observations with an azimuth around 0 or 360° (north of the facula) lie above this line (see **Fig. 3**). Therefore, the radius will be smaller in the south than in the north. Nathair Facula is the only one for which we were able to measure an asymmetry.

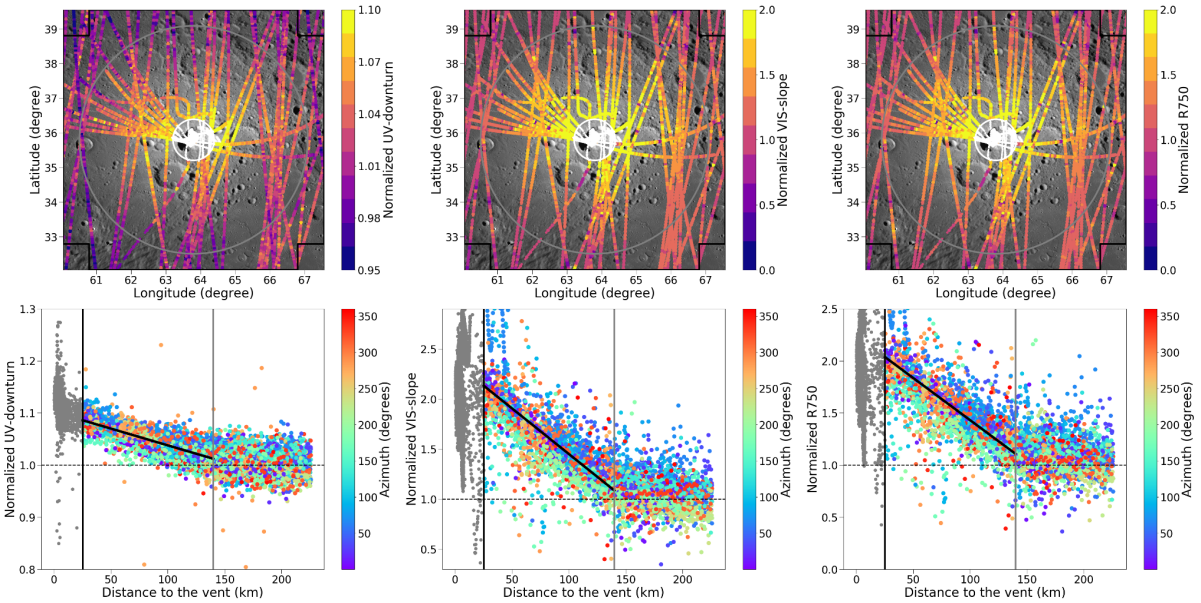

Figure 3: *Variability of the spectral parameters in Nathair Facula. The selected area is a 200 km square and the significance level is 5. The top three panels represent plan views with footprints color-coded based on the strength of normalized spectral parameters. North is up, corresponding to azimuth 0° or 360°. The background map is the Basemap Reduced Data Record (BDR) from Mercury Dual Imaging System (166 m/pixel, Denevi et al., 2018). The black squares at the corners indicate the region used to define the local spectral properties and normalize the parameters. The lower three panels display the evolution of each spectral criterion with respect to distance from the vent centre, color-coded based on the geographical azimuth from the vent centre. The white and grey circles in the top panels, and the corresponding vertical lines in the lower panels, indicate respectively the limit of the vent and the limit of the facula calculated in this work.The black line in each of the bottom plots is a linear regression line. Points within the circle encompassing the vent were excluded from the regression analysis.*

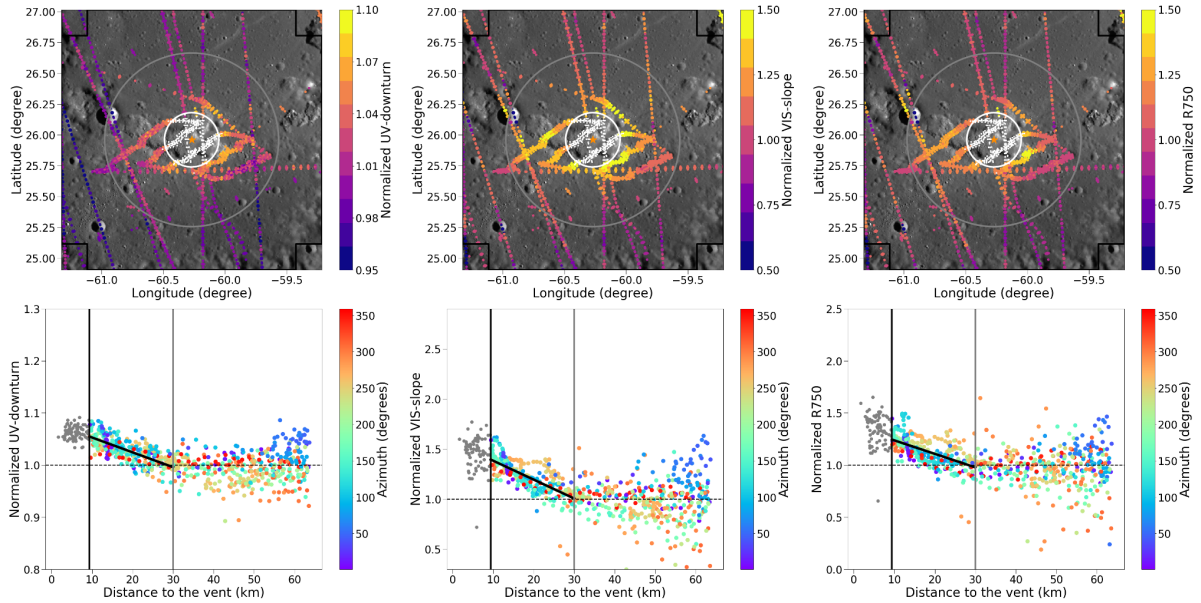

Figure 4: *Variability of the spectral parameters around the pit n°5 (Table 3) in Orm Faculae located within Praxiteles impact crater, presented in the same way as* ***Fig. 3****. The significance level is 4.*

3.1.2. Spectral measurement of facula size

The measured faculae are located over a latitudinal range between 60°S and 50°N and a longitudinal range between -165°E and 160°E. About three quarters of the measured faculae are located in impact craters. The analysis done here made it possible to refine, by including all data available, the radius calculated by previous analyses (Besse et al, (2020), Kerber et al., 2011). Slang Facula in the eastern part of the Caloris basin, which has a significance level of 2, was excluded from this analysis for reasons of global consistency in the spectral treatment between faculae (number and distribution of the data). Suge Facula was also excluded since it is categorized as a Red Pitted Ground by Thomas et al. (2014b). This texture is believed to arise from the sublimation of a volatile species within a young volcanic unit, rather than a primary volcanic explosion (Thomas et al., 2014b; Jozwiak et al., 2018). Of the 12 remaining faculae radii estimated by Besse et al. (2020), 7 were confirmed within a ± 5 km range and 5 were reassessed upwards (by up to 12.5 km). Direct comparison of the extent measured in this study and area measured with multispectral data (MDIS) is complicated since the methodology is different. Kerber et al. (2011) assumed that the facula was circular and centred on the volcanic vent and defined a radius, which is not the case in Thomas et al. (2014b) where they defined the area of the facula. Among the deposits analyzed by Kerber et al (2011), 80% have a radius that was reassessed upwards in this study by more than 5 km. The average faculae radius increase is about 17 km (78 % of the initial radius). The maximum reassessment is 24 km excluding Nathair Facula for which the radius is doubled. Assuming that the MASCS uncertainty is around 500 km² (10-12 km radius), 93% of the deposits measured here cover a larger area than estimated by Kerber et al. (2011) and 55% compared to the areas estimated by Thomas et al. (2014b). However, direct comparison should be treated with caution as the areas determined by Thomas et al. (2014b) are not circular and sometimes contain several deposits in a single measurement. Seven faculae detected in Thomas et al. (2014b) have their radii determined for the first time in this study (**Table. 3**). A facula around the pit within the Neruda impact crater has been identified in this study (**Fig. 5**). The radius of the facula is estimated at 40 km. However, this facula was not mapped in multispectral analyses Kerber et al., (2011) and Thomas et al. (2014b). The geographical locations of the faculae and their dimensions are not related. There is no correlation between radius of the faculae and crater host properties (diameter and degradation class) or vent size.

Table 3: *Pits interpreted as volcanic vents with measurable faculae interpreted as pyroclastic deposit.*

ID (Kerber et al., 2011; Jozwiak et al., 2018; Besse et al., 2020; Thomas et al., 2014b)					Host crater			Volcanic vent			Radius (km)			Deposit Area (km²)			
					Crater/Facula Name	Diameter (km)	Degradation class	Central latitude (°N)	Central longitude (°E)	Area (km²)	Kerber et al., (2011)	Besse et al., (2020)	MASCS - This study (± 5km)	Kerber et al., (2011)	Thomas et al. (2014b)	MASCS - This study	SL
1	K18	J28	B8	T1042	Mistral SE	100,9	2	4,2	-54,03	314,16	19	19	30	1 245	2 548,53	2 827	5
2	K33	J27		T1043	Mistral NW	45,8	3	5,41	-55,8	88,2	11		25	421	2847,89	1 963	5
3	K7	J30	B9	T1045	Lermontov NE	160,9	4	15,79	-48,09	111,3	33	40	45	3 806		6 362	3
4	K9		B10	T1045	Lermontov SW	160,9	4	15,1	-49,1	662,3	31	45	55	3 174	9743,43	9 503	4
5	K19		B13	T1047	Praxiteles SW/Orm	198	N/C	25,96	-60,27	276,6	18	28	30	1 210		2 827	4
6	K11			T1047	Praxiteles NE/Orm	198	N/C	26,85	-59,05	503,6	26		30	2 594	11483,93	2 827	4
7		J48		T5085	No name 1	-	-	-49,8	10,6	99,4			30		2182,92	2 827	4
8	K1	J60	B1	T5082	Rachmaninoff/Nathair	-	-	35,8	63,8	897,11	70	140	140	19 466	38589,11	61 575	5
9		J50		T5092	No name 2	-	-	-53,01	17,71	83			45		3229,815	6 362	5
10	K5	J90	B11	T6062	Caloris/Agwo	1532	3	22,34	146,1	700	24	35	45	4 063	2507,63	6 362	5
11	K28	J89		T6062	Caloris/RS-03 SW	1532	3	21,7	145,49	900	19		35	875	1171,81	3 848	4
12	K20			T6067	Caloris/RS-04 b	1532	3	16,65	156,91	8,64	20		25	1 196	3027,83	1 963	3
13				T6075	Neruda	112	N/C	-52,56	125,65	65,11			40		0	5 027	5
14	K40	J88		T6127	Unnamed crater 5c	-	-	-56,34	143,9	51,6			30		3062,24	2 827	5
15		J15		T7074	No name 3	39,4	N/C	-3,56	-136,87	598			60		23 181,08	11 310	5
16				T7019	No name 4	-	-	-21,09	-162,92	50			20		4089,25	1 257	5
17	K29	J19		T7125	Glinka	93,5	2	14,95	-112,5	195,9	16		25	846	1730,98	1 963	5
18		J25		T7146	No name 5	21,4	N/C	8,59	-68	33,8			25		1820,98	1 963	5
19				T7160	No name 6	66	N/C	-22,86	-90,65	867,3			45		4 214,86	6 362	5
20	K22	J32		T8008	Enheduanna (NE Derzhavin)	108,1	2	48,33	-34	667	15		35	1 111	1875,55	3 848	4
21	K16	J37	B14	T8167	Geddes	85	3	27,05	-29,59	468,3	21	27	30	1 654	2 331,53	2 827	3
22	K4	J34	B3	T8020	Hesiod/Pampu	91,3	2	-57.2	-31.72	22,92	30	40	45	4950		6 362	5
23	K14	J36	B4	T8198	Hesiod/Ular	-	-	-55,1	-30,01	224,5	19	30	40	2079	4363,34	5 027	5
24	K13	J35	B5	T8199	Hesiod/Sarpa	33,7	N/C	-53,04	-30,82	61,5	21	30	35	2233	2957,22	3 848	5
25	K32	J38	B6	T8178	Hesiod/Havu	-	-	-52,34	-28,47	40	9	20	20	453		1 257	5
26	K24		B7	T8178	Hesiod/Bitin	15	N/C	-51,66	-27,86	28,13	14	22,5	35	1021	4363,34	3 848	5

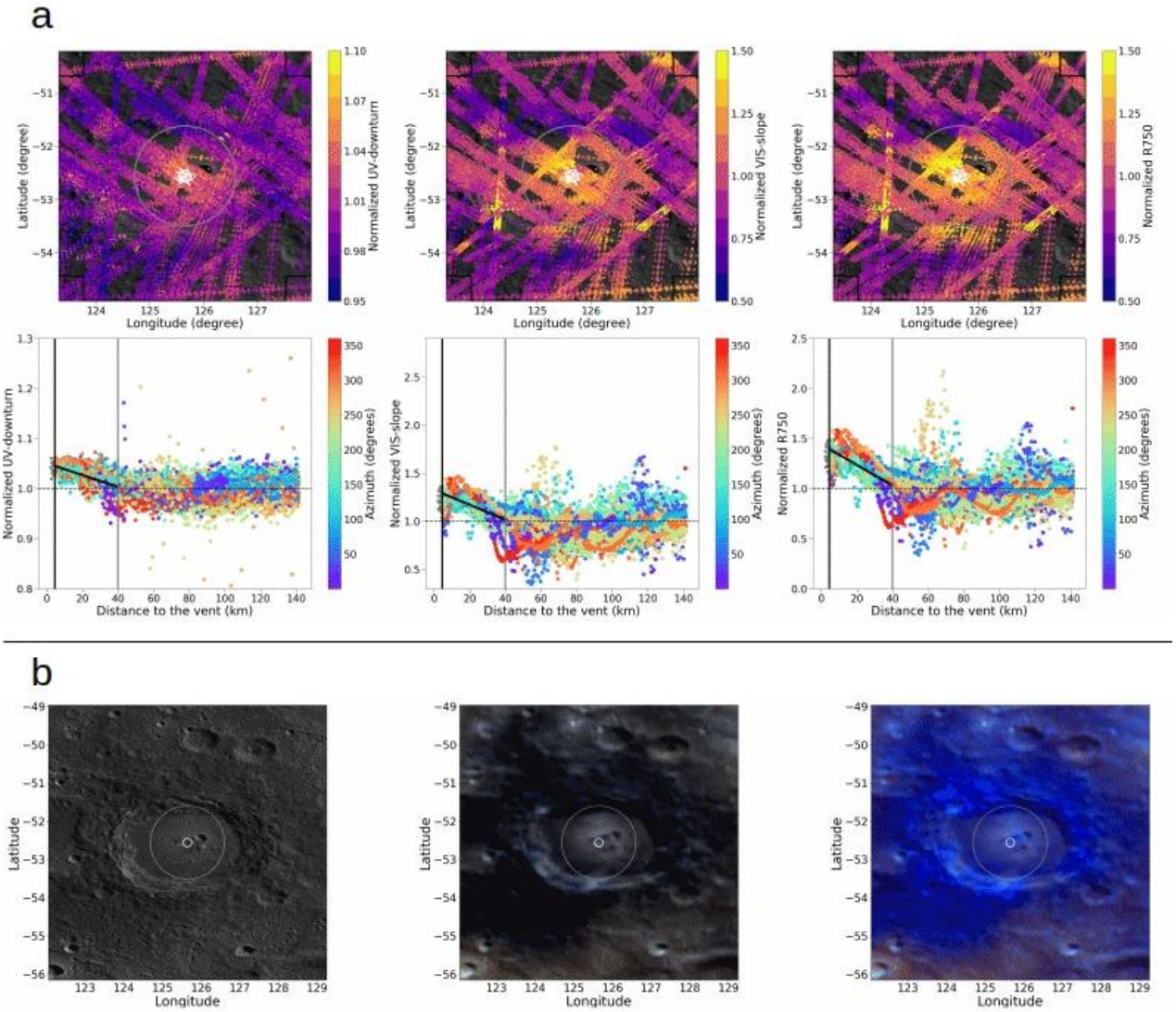

Figure 5: *Comparison between MASCS and MDIS data. a) Variability of the spectral parameters around the pit n°13 (**Table 3**) within Neruda impact crater, presented in the same way as **Fig. 3**. b) MDIS monochrome mosaic (left, 166 m/pixel), 3-color mosaïc (center, R:1000 nm, G:750 nm and B:430 nm, 665 m/pixel) and enhanced color mosaïc (right, R:second principal component, G:first principal component, and B:430/1000 nm ratio, 665 m/pixel) of the Neruda impact crater. The mosaics are from Denevi et al., (2018).*

3.1.3. Implication of faculae's size reassessment on volatiles contents

The presence of volatiles within the interior of Mercury sufficient to drive explosive eruptions has crucial implications for the planet's formation scenario and its geochemical, physical and thermal evolution. The dominant volatiles expected to drive volcanic eruptions would depend on the initial composition of the planet, the reduction state of the mantle and the temperature and pressure conditions encountered during the rise of the erupting magma (Kerber et al., 2011). Volatile species commonly encountered on Earth's magmas are H_2O, CO_2, SO_2, H_2S and HCl. In the chemical conditions of the mantle of Mercury, a combination of more reduced species is expected. Chemical equilibrium models suggest that CO, N_2, S_2, CS_2, S_2Cl, Cl, Cl_2 and COS may be among the most abundant volcanic gases on the planet (Zolotov, 2011). MESSENGER's XRS (X-ray spectrometer) and neutron spectrometer observations show that Nathair Facula is depleted in S and C compared with the rest of the surface (Weider et al., 2016). The authors interpreted this observation as the result of pyroclastic eruptions driven by volatiles originating from oxidation of graphite and/or sulfides in the subsurface magma (Weider et al., 2016). Kerber et al., (2011) estimated abundances of CO, H_2O, CO_2 SO_2 and H_2S needed to create the pyroclastic deposits that they

measured on the surface of Mercury. The horizontal distance reached by any ballistic particle is directly proportional to the released magma gas fraction (Wilson 1980, Kerber et al. 2011). Wilson et Head (1981) determined that approximately 500 ppm of CO (eruption speed of 90 m/s) would be needed to emplace pyroclasts to a distance of 5 km on the Moon. It would take 2.3 times the amount of a particular volatile species to emplace to the same distance on Mercury due to the difference in gravitational acceleration at the surface (Kerber et al., 2011). Following the same approach, we converted the equivalent proportion of volatiles needed to eject a pyroclast particle to the distance given by our faculae radii on Mercury. The volatile content obtained with this approach is based on the assumption that the measured facula was emplaced by a single event. However, if the vent is compound, as is likely on Mercury (Rothery et al., 2014, Pegg et al., 2021), the ballistic range from each eruption can be somewhat smaller than implied by the radius of the facula as a whole. On the other hand, if a facula is the result of one large event creating a deposit with the extent of the facula and several other small events creating multiple small faculae superimposed on the largest, the volatile content calculated here will be a minimum value. Results and comparison with the previously determined abundances of CO and H_2S (Kerber et al., 2011) are displayed in **Fig.6.**

Because the volatile content is proportional to the size of the faculae, the volatile content is, like the radii, increased on average by 78% compared to Kerber et al., (2011). The faculae reassessed here, if correctly interpreted as pyroclastic in origin, imply average volatile contents of 0.9 wt% CO, 1.4 wt% CO_2, 0.6 wt% H_2O, 1.1 wt% H_2S or 2.1 w% SO_2 (**Table S2**). The spatial resolution of MASCS does not allow the study faculae smaller than 500 km^2, so the average volatile content expressed here could be revised with future BepiColombo observations. Volatile contents of some arc and back-arc basaltic magmas on Earth, measured in melt inclusions, vary from 0.1 to 8 wt% H_2O, 0 to 2100 ppm CO_2 and 300-6000 ppm S (Wallace 2005). Melt inclusions from explosive deposits of the Bishop Tuff (Wallace et al., 1999), the Tuff of Pine Grove (Lowenstern et al., 1994), Mount Pinatubo (Wallace and Gerlach 1994) and Altiplano-Puna volcanic complex (Schmitt, 2001) reveal CO_2 contents that range from 10 to 1085 ppm and water contents between 2.8 wt% and 7 wt%. H_2O contents measured on Earth are comparable (basaltic magma) or higher (rhyolitic magma) than those measured on Mercury. However, the highest values are from subduction settings where partial melting of the mantle is generated by the addition of water from the subducted oceanic crust into the mantle; such a process is unlikely to be comparable with those on Mercury. The actual gas driving the pyroclastic eruptions on Mercury will most likely be a combination of several volatiles, including S and C (Weider et al., 2016). CO_2 contents on Earth are lower than those necessary for the formation of faculae on Mercury. In particular for the extreme case of Nathair Facula where the CO_2 content, assuming that it is the only gas at the origin of the eruption, is up to an order of magnitude higher than those measured on Earth. The size of the faculae and the resulting volatile contents in magmas support the point that Mercury's interior is far more enriched in volatile species than had been thought. Such a result may favor a formation history that allows for the accretion of volatile-rich planetesimals (Kerber et al., 2009) or perhaps the consequence of magma storage in the shallow subsurface (Thomas et al., 2014b).

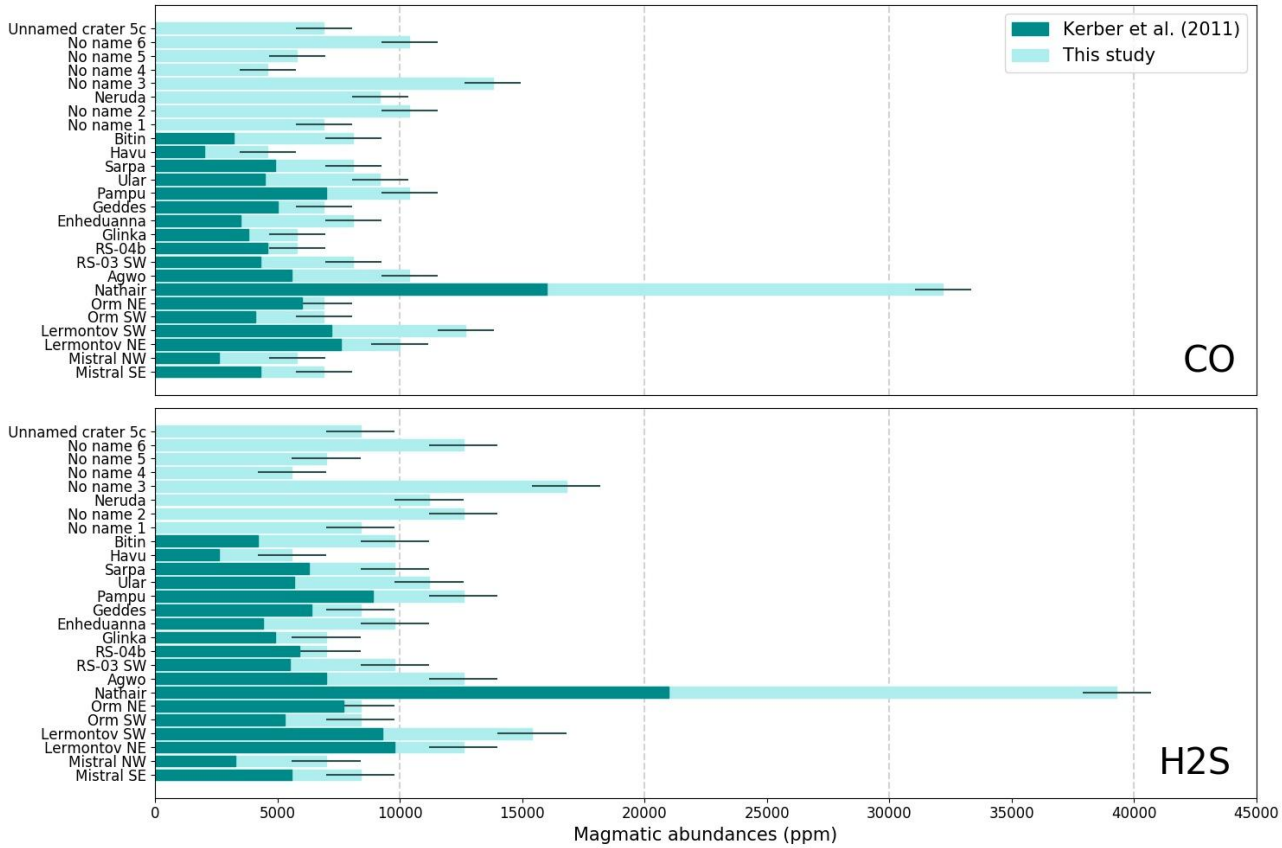

Figure 6: *Magmatic content of CO (top) or H_2S (bottom) needed to form the measured faculae on Mercury, under the assumption that CO or H_2S was the only driving volatile. The error bars, related to the uncertainty to the radius (± 5 km), correspond to 1150 ppm CO and 1400 ppm H_2S.*

3.2. Spectral variability of the faculae

Goudge et al. (2014) emphasized the spectral variability between faculae in the near-ultraviolet to visible. In order to better investigate this variability, the spectral properties of the 26 measured faculae are compared together. However, this work should be done carefully since the spectral parameters change as a function of distance to the vent. A way to minimize the issue due to this intrinsic variability is to take the spectral properties of the faculae at a similar location from their vents (Besse et al., 2015). As in Besse et al., (2020), the spectral properties of the faculae are taken at the midpoint between the limit of the vent and edges of the facula. In order to compare the spectral properties of the faculae at global scale, the values of the spectral parameters are no longer normalized by the local mean.

The fact of not reducing the analysis to 3 MASCS orbits and thus increasing considerably the number of observations for the faculae has slightly modified the values of the spectral parameters in the near-UV to visible already calculated by Besse et al. (2020) (**Fig.7**). However, the range of UV-downturn and VIS-slope of these faculae remains globally the same (see black rectangle in **Fig. 7**). By increasing the sample studied (12 to 26), the spectral variability of the faculae also increased. Previously, Besse et al. (2020) mentioned that the faculae were easily distinguishable from the mean surface of Mercury thanks to their VIS-slope and UV-downturn always respectively higher than 1 or 3.1. This characteristic is no longer valid since the faculae located in Neruda, Unnamed crater 5c and Enheduanna impact craters and the faculae named “No name 4” have a VIS-slope lower than 1. The UV-downturn remains higher than 3.1 for the faculae except for the facula in Neruda impact crater which has a UV-downturn egal to 3.1.

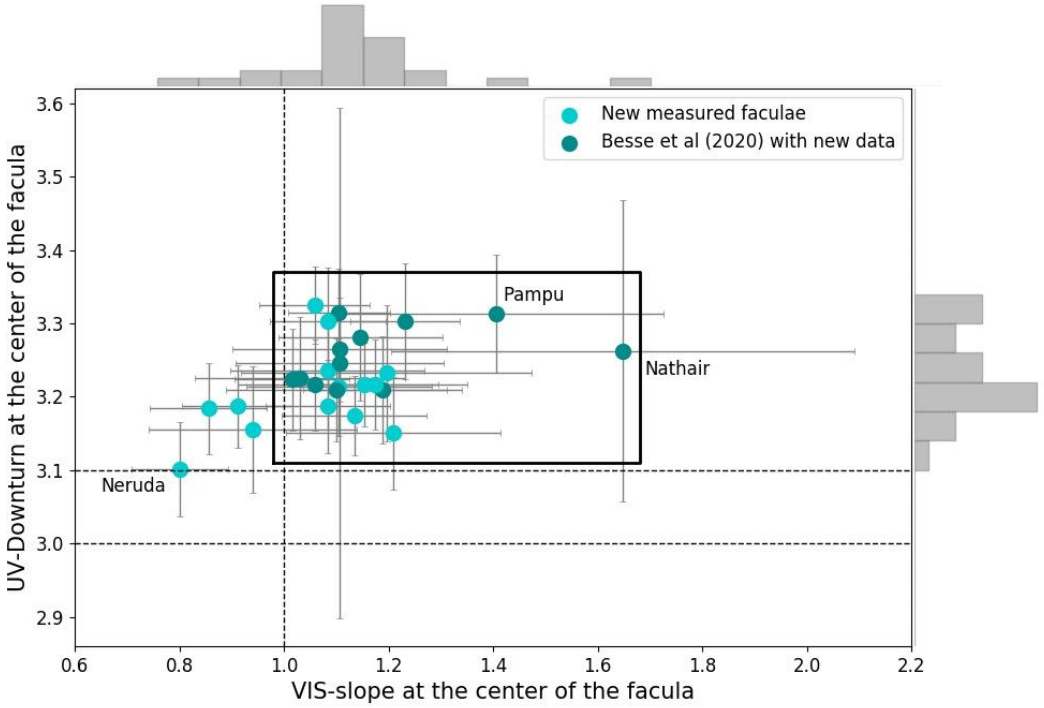

Figure 7: *UV-downturn versus VIS-slope at the midpoint of the 26 measured faculae. The spectral parameters are absolute values and are not normalized by the local mean. The bars represent the standard deviation of all the MASCS observations in each facula. Histograms show the distribution of the data within the diagram. The black dashed lines at 3.0 and 3.1 respectively represent the Mercury mean spectrum (Izenberg et al., 2014) and an averaged floor spectra of the Hesiod region (Besse et al., 2020). The black rectangle shows the range of values in figure 6 of Besse et al. (2020).*

The faculae are not systematically brighter (at the midpoint of the deposit) than the average surface of Mercury. The parameters R750 (**Fig. 8a**) and R575 are in several cases lower than the value of the reference spectrum of Mercury. Finally, what differentiates the pyroclastic deposits are their spectral properties in relation to the local spectral properties, i.e. the surrounding terrain.

For most of the faculae, the UV-downturn ranges, at the midpoint, between 3.15 and 3.35 (**Fig. 8**), the VIS-slope between 0.8 to 1.2 and the R750 between 0.04 and 0.06. Nathair Facula with a R750 and VIS-slope parameters, at the midpoint of the facula, of respectively 0.072 and 1.65 appears as an end member in the visible. The facula in the Neruda impact crater is also an endmember, with the minimum value of VIS-slope, R750 and UV-downturn. These low values compared to the other faculae could explain why the facula was not mapped with the MDIS data.

The spectral properties of the faculae are not correlated with other parameters such as geographic location, size of the facula, diameter of the crater host and size of the vent. In particular, the spectral parameters are not related to the degradation class of the host craters, which fixes an upper limit on the age of the faculae. Space-weathering affects spectral properties of lunar soils by darkening and reddening the spectrum at visible to near-infrared wavelengths (McCord and Adams 1973; Fischer and Pieters 1994). However, recents study (Jozwiak et al., 2021) of vent morphologies reveals that the most degraded vents on Mercury are not constrained to the most degraded host craters. A comparison between vents degradation class and spectral properties of faculae seems therefore more appropriate to determine the contribution of space-weathering to the spectral properties of faculae.

The faculae that are located within the same impact crater present very close values of spectral parameters (**Fig. 8**). The vents in the Lermontov impact crater are separated by about 60 km. However the radii of the faculae around each of these vents are 55 and 45 km (**Table 3**). Thus, the faculae could be superimposed in some places, contributing mutually to the spectral properties of the other. However, this hypothesis is refuted for the faculae within the Caloris basin and Praxiteles

impact crater. The vents of RS-03 SW and Agwo Facula are located about 40 km from each other. Since the faculae have radii of 35 and 45 km, mixing between the two may well have occurred. But in the case of RS-04b, the facula cannot be superimposed on the other two because the pits are separated by about 500 km. The close spectral properties of Agwo, RS-03 SW, and RS-04b are therefore not due to a mixing between the faculae.

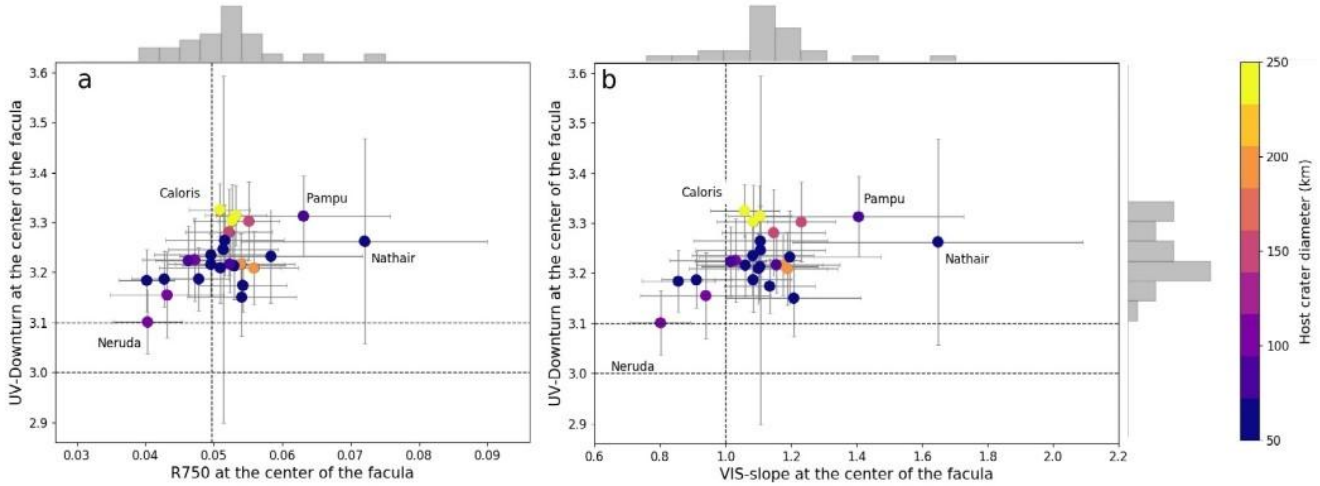

Figure 8: *Parameter spaces for the 26 measured faculae in the visible and ultraviolet domains. The values of the spectral parameters are absolute and are not normalized by the local mean. The black dashed lines represent the Mercury mean spectrum (Izenberg et al., 2014). The bars represent the standard deviation of the MASCS observations in each facula. The color code represents the host crater diameter (km). Histograms show the distribution of the data within the diagrams. The three yellow dots correspond to deposits located in Caloris basin, the two orange and the two pink/red are the deposits located respectively in Praxiteles and Lermontov impact craters. a) UV-downturn versus R750 at the midpoint of the facula. b) UV-Downturn versus VIS-slope at the midpoint of the facula. The R750 and the VIS-slope are linearly correlated (Pearson coefficient correlation of 0.98, at 99.9%) but it may be related to the mathematical definition and the overlapping wavelength range between the parameters.*

4. Discussion

4.1. Fraction of juvenile magma in faculae

The similarity in spectral properties between faculae in the same impact crater (**Fig. 8**) could be explained by (1) the composition of the magma or (2) by large contribution of the country rocks in spectral properties.

The closed spectral properties of the faculae in the same host crater could be the result of a similar magmatic source producing faculae with the same composition. For example, lunar pyroclastic deposits in Lavoisier (70 km in diameter) and Lavoisier F impact craters share similar spectral features, indicating similar mineralogical compositions and possibly the same volcanic origin (Souchon et al, 2013). Here, we propose, for Caloris basin, Praxiteles and Lermontov impact craters that a dike propagates to a shallow subsurface, forms a sill/laccolith leading to several other dikes propagating to the surface and generating pyroclastic features. In the case of the Caloris basin, where the faculae are separated by 500 km, the laccolith does not need to extend over similar dimensions. Globally the lithosphere of Mercury has been under a contractional tectonic regime for most of its history (Byrne et al., 2014). Under contractional tectonic regimes, magma preferentially migrates horizontally to form sills and laccolith rather than vertically (Sibson et al., 2003). If the magma ascends along pre-existing weaknesses in the lithosphere, such as thrust fault and fractures associated with impact structures (Caloris basin), magma propagation is not necessarily vertical.
The three deposits analyzed in the Caloris Basin (RS-03b, Agwo and RS-04b) have different volatile content, ranging from 5800 to 10400 ppm CO (**Fig 6**). On Earth, it is observed that different content in volatiles can be achieved by fractional crystallization during magma storage at shallow

levels (Fowler and Spera, 2008). The three Caloris deposits could therefore have been emplaced at different times (different degrees of fractional crystallization), explaining why they have different volatile contents. However, fractional crystallization implies different mineralogical compositions between the lava forming the three faculae. In this case, a spectral difference could be observed. Moreover, on the Moon, formation of sill/laccolith produces an uplifted/domed floor and concentric and/or radial floor fractures. This is the formation mechanism of lunar floor fractured craters and Lavoisier impact crater is one of them (Schultz, 1976, Jozwiak et al, 2012). On Mercury, there is no evidence for such craters that host pyroclastic vents. The Caloris basin hosts an extensional system composed of a radial fracture network, Pantheon fossae, which may be formed in response to upwelling beneath the basin (Head et al., 2009). However, Klimczak et al., (2010) demonstrated that the graben are not consistent with intrusive magmatic formation. Based on these arguments and morphological analyzes, Jozwiak et al., (2018) suggested a dike-venting model as formation geometry for the majority of hermean pyroclastic vents.

The spectral similarities between faculae in the same impact crater may also be due to a low fractions of juvenile (magmatic) material in the faculae. If the magmatic sources and/or the magmatic differentiation (fractional crystallization during magma storage) are different for faculae in the same impact crater, their similarities in spectral properties could be due to the fraction of country rocks. The mixing between juvenile and country rock materials could occur in several ways: during magma ascent, during emplacement of ballistic particles, and/or after pyroclastic emplacement by impact cratering and gardening. The proportion of non juvenile material in the faculae could vary a lot. The juvenile magma may be mainly composed of gas and a very small amount of melt. In this case, the faculae will be mostly composed of country rocks fragmented during the eruption of high-velocity rising gas. The spectral contrast with the surroundings will therefore be due to the physical properties of the material such as grain size rather than compositional differences. Phase-ratio images of Agwo faculae reveal that the pyroclastic deposit is characterized by smoother sub-resolution texture or smaller particles than adjacent background terrain (Blewett et al., 2014). Topographic data (Thomas et al., 2014b) and modelling (Bröz et al., 2018) suggested that faculae are composed of a very gentle blanket of pyroclasts. Thus, the high volatile content and the possible limited eruption volume support the hypothesis of a low fraction of juvenile magma compared to country rocks in faculae. In addition, the facula in the Neruda impact crater (**Fig 5**) with the lowest values of VIS-slope, UV-downturn and R750 (**Fig. 8**) is in a representative area of LRM (Klima et al., 2018). LRM is known to have values of R750, UV-downturn and VIS-slope parameters generally lower than Mercury's mean surface (Barraud et al., 2020). This also reinforces the hypothesis of a low proportion of juvenile magma in the facula compared to the proportion of country rocks contributing predominantly to its spectral properties.

4.2. Eruptive style

Mercury’s pits are incised into bedrock and are surrounded by low-relief deposits. Based on these morphological characteristics, Thomas et al. (2014b) suggested that hermean pits and deposits are similar to maars on Earth resulting from phreatomagmatic eruption (interaction between rising magma and non magmatic volatiles). The XRS and GNRS measurements revealed that the surface of Mercury is volatiles-rich, in particular with relatively high abundances of S and C (Nittler et al., 2011). Thus, the hypothesis that Mercury’s explosive features are formed by a process comparable to phreatomagmatism seems compatible. Hermean phreatomagmatic eruption may be involved by interaction between rising magma and S or C-rich layer.

Phreatomagmatic events are characterized by high degree of explosivity, wide dispersal of deposits, and high degree of fragmentation of the lava (Walker, 1973). Nathair Facula is the most widely dispersed faculae on the surface of Mercury (**Table 3**). In addition to its dimensions, Nathair Facula appears as an end-member in terms of spectral parameters (**Fig. 8**). Its high reflectance value at 750 nm could be explained by a difference of physical properties. Indeed, when the grain size decreases the reflectance increases (Crown and Pieters, 1987). On Earth, the proportion of pyroclasts with a size lower than 1 mm in phreatomagmatic products can reach 100%. Thus, we propose that Nathair Facula is the result of phreatomagmatic-like events having caused wider dispersion and higher degree fragmentation of the material than for the other faculae. In many terrestrial maar formations, the country rock is the predominant constituent of the erupted mass

where the juvenil material makes up a small portion (White and Ross, 2011). Therefore, the Nathair Facula formation hypothesis is consistent with our earlier hypothesis that the faculae on Mercury's surface could consist of a large portion of country rocks.

A difference in elemental composition is observed between the Nathair Facula and its surrounding terrain; the facula is depleted in S and C (Weider et al, 2016). However, this difference may be, as originally reported by Thomas et al. (2014b), induced by the loss of volatile elements rather than by a compositional difference with the country rocks. If the formation of the explosive features (vent and facula) occurs by interaction between hot-magma and initially sulfur- and/or carbon-rich country rock, sulfur or carbon may have been changed to gaseous compounds during the eruption.

LRM regions measured by neutron spectroscopy (Peplowski et al., 2016) are carbon-rich compared to Mercury's mean surface. Mercury's extreme mantle composition may have led to primary graphite flotation crust production that was subsequently covered by secondary magmas (Vander Kaaden et al., 2015). This graphite layer would then be excavated on the surface by impact events forming the visible LRM. Klima et al., (2018) reported a relationship between a 600-nm band depth observed in multispectral MDIS data and carbon content as derived from neutron spectroscopy measurements, which can be used to estimate carbon enrichment of LRM. Typical LRM exposures contain an excess of 2–2.5 wt% carbon but LRM related to Basho and Rachmaninoff craters have higher excess carbon (>4 wt%, perhaps up to 4.5 wt%) (Klima et al., 2018). Nathair Facula lies about 200 km beyond the northeast rim of the Rachmaninoff crater. Therefore, the ascent of a magma at this location where the subsurface seems unusually rich in carbon may have generated a phreatomagmatic eruption. This result explains why Nathair Facula is an end-member in terms of spectral properties, dimensions and volatile content. The magmas at the origin of the other pyroclastic deposits on the surface of Mercury would not have crossed a layer as rich as the one present at the Rachmaninoff crater, leading to such a high energetic eruption.

5. Conclusions

The results of the spectral investigation of Mercury’s pit's surroundings with MASCS/MESSENGER are:

- At least 25 % of the pits are related to faculae. Using the linear decrease of three spectral parameters: the UV-downturn, the slope in the visible and the reflectance at 750 nm, we estimated the radius of 26 faculae. 80 % of the radii were reassessed upwards in this study by more than 5 km (on average 17 km). As the radius, estimates of the volatile contents needed to emplace faculae were on average reassessed upwards by 78 % from previous analysis. The volatile mass fractions are in many cases comparable or greater than those found in explosive products on Earth. Although it is admitted today that Mercury is not depleted in volatiles as thought before MESSENGER, the explosive activity of the planet seems to have been underestimated.

- The spectral properties of faculae located in the same host crater are relatively similar suggesting that these faculae are dominated by country rocks. Magmas at the origin of the Hermean explosive eruptions may be mainly composed of gas with a small fraction of melt. Faculae are not always brighter and redder than Mercury's mean surface but rather than their local surroundings. The difference in spectral properties between faculae and country rocks could be related to variations of grain size between fragmented and not fragmented country rocks, or as in the case of Nathair Facula by volatilization of sulfur-rich and/or carbon-rich substrates.

- The extreme spectral properties of Nathair Facula, especially in the visible, could be induced by a high degree of fragmentation of the pyroclasts, characteristic of a phreatomagmatic-like process. Moreover, the widely dispersed deposit and the extreme volatile content of Nathair Facula are consistent with phreatomagmatic events, produced by interaction between hot magma and a possible subsurface layer locally enriched in carbon. This hypothesis is in agreement with our proposition that country rocks are predominant in

faculae on Mercury, since the phreatomagmatic products on Earth are composed of a small portion of juvenil material.

Our analysis also revealed that the low spatial coverage of MASCS is an important shortcoming for the study of explosive volcanism from a spectral point of view as 60% of the pits' surroundings are not covered or not covered enough to be studied consistently with MASCS. Future observations with BepiColombo should certainly solve some of these issues. The global coverage at 480 m/pixel by the hyperspectral imager VIHI (Visual and Infrared Hyperspectral Imager) from the instrumental suite SIMBIO-SYS (Spectrometer and Imaging for MPO BepiColombo Integrated Observatory SYStem; Cremonese et al., 2020) will allow a detailed spectral analysis of a larger sample of faculae. It would be useful, with future observations of SIMBIO-SYS at different phase angles and of the MERTIS (Mercury Radiometer and Thermal Infrared Spectrometer, Hiesinger et al., 2010) spectrometer, to define the degree of fragmentation of the material constituting the faculae, in order to better constrain the eruptive style. Moreover, determination of composition, volume and volcanic glass content of the faculae using a combination of measurements from VIHI, MERTIS, the BepiColombo Laser Altimeter (BELA), the Gamma-Ray and Neutron Spectrometer (MGNS) and the Mercury Imaging X-Ray spectrometer (MIXS) should provide important constraints on Hermean's explosive activity (Rothery et al., 2020).

Data availability

The data used in this work are available at the PDS Geosciences Node of Washington University, St. Louis, MO, USA. The dataset used contains the latest calibration provided by the MESSENGER science team. (https://pds-geosciences.wustl.edu/messenger/mess-e_v_h-mascs-3-virs-cdr-calda-ta-v1/messmas_2101/data/ddr/)

Acknowledgements

The authors thank the two anonymous referees for helpful comments at the review stage. The authors acknowledge the Centre National des Etudes Spatiales (CNES) for continuous and long term support. O. Barraud acknowledges the support of the European Space Astronomy Centre (ESAC) faculty council for funding a visit to ESAC as part of this work.

References:

Barraud, O., Doressoundiram, A., Besse, S., & Sunshine, J. M. (2020). Near-ultraviolet to near-infrared spectral properties of hollows on Mercury: Implications for origin and formation process. *Journal of Geophysical Research: Planets*, *125*(12), e2020JE006497.

Besse, S., A. Doressoundiram, and J. Benkhoff (2015), Spectroscopic properties of explosive volcanism within the Caloris basin with MESSENGER observations, *J. Geophys. Res. Planets*, 120, doi:10.1002/2015JE004819.

Besse, S., Doressoundiram, A., Barraud, O., Griton, L., Cornet, T., Munoz, C., et al. (2020). Spectral properties and physical extent of pyroclastic deposits on Mercury: Variability within selected deposits and implications for explosive volcanism. *Journal of Geophysical Research: Planets*, 125, e2018JE005879.

Blewett, D. T., Levy, C. L., Chabot, N. L., Denevi, B. W., Ernst, C. M., & Murchie, S. L. (2014). Phase-ratio images of the surface of Mercury: Evidence for differences in sub-resolution texture. *Icarus*, *242*, 142-148.

Brož, P., Čadek, O., Wright, J., & Rothery, D. A. (2018). The Apparent Absence of Kilometer-Sized Pyroclastic Volcanoes on Mercury: Are We Looking Right?. *Geophysical Research Letters*, *45*(22), 12-171.

Byrne, P. K., Whitten, J. L., Klimczak, C., McCubbin, F. M., & Ostrach, L. (2019). The volcanic character of Mercury.

Byrne, P. K., Klimczak, C., Şengör, A. C., Solomon, S. C., Watters, T. R., & Hauck, S. A. (2014). Mercury's global contraction much greater than earlier estimates. *Nature Geoscience*, *7*(4), 301-307.

Cremonese, G., Capaccioni, F., Capria, M. T., Doressoundiram, A., Palumbo, P., Vincendon, M., ... & Turrini, D. (2020). SIMBIO-SYS: Scientific Cameras and Spectrometer for the BepiColombo Mission. *Space science reviews*, *216*(5), 1-78

Crown, D. A., & Pieters, C. M. (1987). Spectral properties of plagioclase and pyroxene mixtures and the interpretation of lunar soil spectra. *Icarus*, *72*(3), 492-506.

Denevi, B. W., Chabot, N. L., Murchie, S. L., Becker, K. J., Blewett, D. T., Domingue, D. L., ... & Solomon, S. C. (2018). Calibration, projection, and final image products of MESSENGER's Mercury Dual Imaging System. *Space Science Reviews*, *214*(1), 1-52.

Fischer, E. M., & Pieters, C. M. (1994). Remote determination of exposure degree and iron concentration of lunar soils using VIS-NIR spectroscopic methods. *Icarus*, *111*(2), 475-488.

Fowler, S. J., and Spera, F. J. (2008), Phase equilibria trigger for explosive volcanic eruptions, *Geophys. Res. Lett.*, 35, L08309, doi:10.1029/2008GL033665.

Goudge, T. A., et al. (2014), Global inventory and characterization of pyroclastic deposits on Mercury: New insights into pyroclastic activity from MESSENGER orbital data, J. Geophys. Res. Planets, 119, 635–658, doi:10.1002/2013JE004480.

Head, J. W., Murchie, S. L., Prockter, L. M., Robinson, M. S., Solomon, S. C., Strom, R. G., ... & Gillis-Davis, J. J. (2008). Volcanism on Mercury: Evidence from the first MESSENGER flyby. *Science*, *321*(5885), 69-7

Head, J. W., Murchie, S. L., Prockter, L. M., Solomon, S. C., Chapman, C. R., Strom, R. G., ... & Kerber, L. (2009). Volcanism on Mercury: Evidence from the first MESSENGER flyby for extrusive and explosive activity and the volcanic origin of plains. *Earth and Planetary Science Letters*, *285*(3-4), 227-242.

Hiesinger, H., Helbert, J., & Team, M. C. I. (2010). The Mercury radiometer and thermal infrared spectrometer (MERTIS) for the BepiColombo mission. *Planetary and Space Science*, *58*(1-2), 144-165.

Izenberg, N. R., Klima, R. L., Murchie, S. L., Blewett, D. T., Holsclaw, G. M., McClintock, W. E., ... & Dyar, M. D. (2014). The low-iron, reduced surface of Mercury as seen in spectral reflectance by MESSENGER. *Icarus*, *228*, 364-374.

Jawin, E. R., S. Besse, L. R. Gaddis, J. M. Sunshine, J. W. Head, and S. Mazrouei (2015), Examining spectral variations in localized lunar dark mantle deposits, J. Geophys. Res. Planets, 120, 1310–1331, doi:10.1002/2014JE004759.

Jozwiak, L. M., Head, J. W., & Wilson, L. (2018). Explosive volcanism on Mercury: Analysis of vent and deposit morphology and modes of eruption. *Icarus*, *302*, 191-212.

Jozwiak, L. M., Head, J. W., Zuber, M. T., Smith, D. E., & Neumann, G. A. (2012). Lunar floor-fractured craters: Classification, distribution, origin and implications for magmatism and shallow crustal structure. *Journal of Geophysical Research: Planets*, *117*(E11).

Jozwiak, L. M., Wagoner, C. M., & Izenberg, N. R. (2021, March). Investigating the Unexpected Youth of Mercury's Pyroclastic Deposits. In *Lunar and Planetary Science Conference* (No. 2548, p. 2223).

Kerber, L., Head, J. W., Solomon, S. C., Murchie, S. L., Blewett, D. T., & Wilson, L. (2009). Explosive volcanic eruptions on Mercury: Eruption conditions, magma volatile content, and implications for interior volatile abundances. *Earth and Planetary Science Letters*, *285*(3-4), 263-271.

Kerber, L., Head, J. W., Blewett, D. T., Solomon, S. C., Wilson, L., Murchie, S. L., ... & Domingue, D. L. (2011). The global distribution of pyroclastic deposits on Mercury: The view from MESSENGER flybys 1–3. *Planetary and Space Science*, *59*(15), 1895-1909.

Klima, R. L., Denevi, B. W., Ernst, C. M., Murchie, S. L., & Peplowski, P. N. (2018). Global distribution and spectral properties of low-reflectance material on Mercury. *Geophysical Research Letters*, *45*(7), 2945-2953.

Klimczak, C., & Byrne, P. K. (2018). Open Questions on the Global Contraction of Mercury. *Mercury: Current and Future Science of the Innermost Planet*, *2047*, 6049.

Klimczak, C., Schultz, R. A., & Nahm, A. L. (2010). Evaluation of the origin hypotheses of Pantheon Fossae, central Caloris basin, Mercury. *Icarus*, *209*(1), 262-270.

Lowenstern, J. B. (1994). Major-element, trace-element, and volatile concentrations in silicate melt inclusions from the tuff of Pine Grove, Wah Wah Mountains, Utah.

McClintock, W. E., & Lankton, M. R. (2007). The Mercury Atmospheric and Surface Composition Spectrometer for the MESSENGER mission. *Space Science Reviews*, 131 (1-4), 481-521. doi: 10.1007/s11214-007-9264-5
McCord, T. B., & Adams, J. B. (1973). Progress in remote optical analysis of lunar surface composition. *The Moon*, *7*(3-4), 453-474.

Nittler, L. R., Starr, R. D., Weider, S. Z., McCoy, T. J., Boynton, W. V., Ebel, D. S., ... & Sprague, A. L. (2011). The major-element composition of Mercury's surface from MESSENGER X-ray spectrometry. *Science*, *333*(6051), 1847-1850.

Pegg, D. L., Rothery, D. A., Balme, M. R., & Conway, S. J. (2021). Explosive vent sites on mercury: Commonplace multiple eruptions and their implications. *Icarus*, 114510.

Peplowski, P. N., Klima, R. L., Lawrence, D. J., Ernst, C. M., Denevi, B. W., Frank, E. A., ... & Solomon, S. C. (2016). Remote sensing evidence for an ancient carbon-bearing crust on Mercury. *Nature Geoscience*, *9*(4), 273-276.

Rothery, D. A., Barraud, O., Besse, S., Carli, C., Pegg, D. L., Wright, J., & Zambon, F. (2021). On the asymmetry of Nathair Facula, Mercury. *Icarus*, *355*, 114180.

Rothery, D. A., Massironi, M., Alemanno, G., Barraud, O., Besse, S., Bott, N., ... & Zambon, F. (2020). Rationale for BepiColombo studies of Mercury's surface and composition. *Space science reviews*, *216*, 1-46.

Rothery, D. A., Thomas, R. J., & Kerber, L. (2014). Prolonged eruptive history of a compound volcano on Mercury: Volcanic and tectonic implications. *Earth and Planetary Science Letters*, *385*, 59-67.

Schmitt, A. K. (2001). Gas-saturated crystallization and degassing in large-volume, crystal-rich dacitic magmas from the Altiplano-Puna, northern Chile. *Journal of Geophysical Research: Solid Earth*, *106*(B12), 30561-30578.

Schultz, P. H. (1976). Floor-fractured lunar craters. *The Moon*, *15*(3-4), 241-273.

Sibson, R. H. (2003). Brittle-failure controls on maximum sustainable overpressure in different tectonic regimes. *AAPG bulletin*, *87*(6), 901-908.

Solomon, S. C., McNutt, R. L., Gold, R. E., & Domingue, D. L. (2007). MESSENGER mission overview. *Space Science Reviews*, *131*(1-4), 3-39.

Souchon, A. L., S. Besse, P. C. Pinet, S. D. Chevrel, Y. H. Daydou, J.-L. Josset, L. D'Uston, and J. Haruyama (2013), Local spectrophotometric properties of pyroclastic deposits at the Lavoisier lunar crater, *Icarus*, 225, 1– 14.

Thomas, R. J., D. A. Rothery, S. J. Conway, and M. Anand (2014a), Long-lived explosive volcanism on Mercury, Geophys. Res. Lett.,41, 6084–6092, doi:10.1002/2014GL061224.

Thomas, R. J., Rothery, D. A., Conway, S. J., and Anand, M. (2014b), Mechanisms of explosive volcanism on Mercury: Implications from its global distribution and morphology, *J. Geophys. Res. Planets*, 119, 2239– 2254, doi:10.1002/2014JE004692.

Thomas, Rebecca (2015). Planet Mercury: volatile release on a contracting world. PhD thesis The Open University.

Vander Kaaden, K. E., & McCubbin, F. M. (2015). Exotic crust formation on Mercury: Consequences of a shallow, FeO-poor mantle. *Journal of Geophysical Research: Planets*, *120*(2), 195-209.

Walker, G.P.L. (1973). Explosive volcanic eruptions — a new classification scheme. *Geol Rundsch* **62,** 431–446 .

Wallace, P.J., (2005), Volatiles in subduction zone magmas: Concentrations and fluxes based on melt inclusion and volatile gas data: Journal of Volcanology and Geothermal Research, v. 140, p. 217–240, doi: 10.1016/j.jvolgeores.2004.07.023.

Wallace, P. J., Anderson Jr, A. T., & Davis, A. M. (1999). Gradients in H2O, CO2, and exsolved gas in a large-volume silicic magma system: Interpreting the record preserved in melt inclusions from the Bishop Tuff. *Journal of Geophysical Research: Solid Earth*, *104*(B9), 20097-20122.

Wallace, P. J., & Gerlach, T. M. (1994). Magmatic vapor source for sulfur dioxide released during volcanic eruptions: evidence from Mount Pinatubo. *Science*, *265*(5171), 497-499.

Weider, S. Z., Nittler, L. R., Murchie, S. L., Peplowski, P. N., McCoy, T. J., Kerber, L., ... & Solomon, S. C. (2016). Evidence from MESSENGER for sulfur-and carbon-driven explosive volcanism on Mercury. *Geophysical Research Letters*, *43*(8), 3653-3661.

White, J. D., & Ross, P. S. (2011). Maar-diatreme volcanoes: A review. *Journal of Volcanology and Geothermal Research, 201(1-4), 1-29.*

Wilson, L. (1980). Relationships between pressure, volatile content and ejecta velocity in three types of volcanic explosion. *Journal of Volcanology and Geothermal Research, 8(2-4), 297-313.*

Wilson, L., & Head, J. W. (1981). Ascent and eruption of basaltic magma on the Earth and Moon. *Journal of Geophysical Research: Solid Earth, 86(B4), 2971-3001.*

Wilson, L., & Head, J. W. (2003). Deep generation of magmatic gas on the Moon and implications for pyroclastic eruptions*. Geophysical Research Letters, 30(12).*

Zolotov, M. Y. (2011). On the chemistry of mantle and magmatic volatiles on Mercury. *Icarus, 212(1), 24-41.*

SUPPLEMENTARY MATERIALS

Spectral investigation of Mercury's pits surroundings: Constraints on the planet's explosive activity

Authors: Océane Barraud[1] (corresponding author), Sébastien Besse[2], Alain Doressoundiram[1], Thomas Cornet[2] and Claudio Munoz[2].

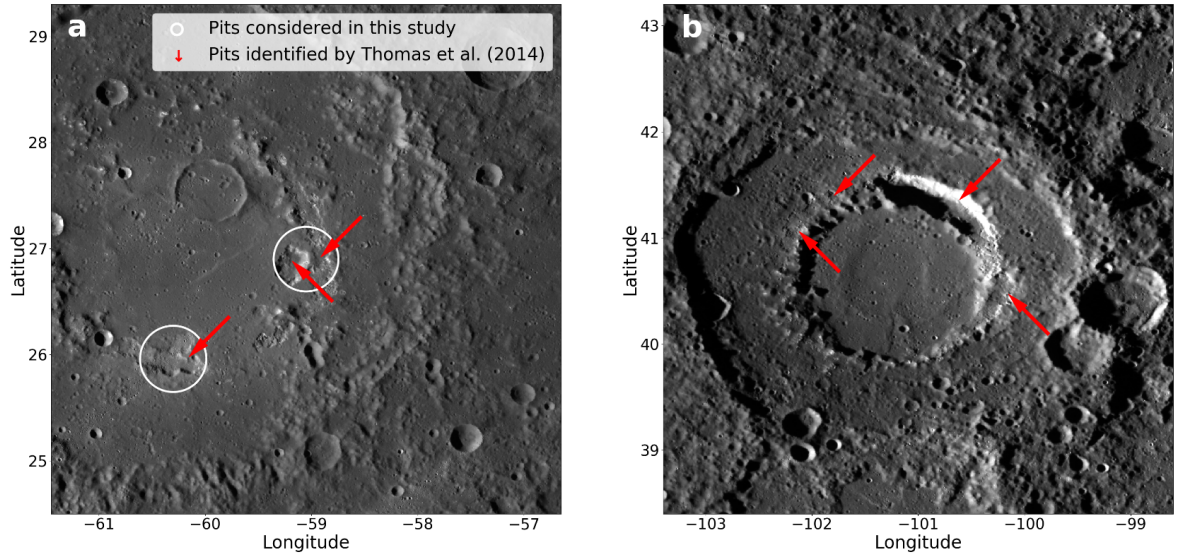

Figure S1: *Examples of pits in Praxiteles (a) and Scarlatti (b) impact craters. (a) The two pits (red arrows) identified by Thomas et al. (2014) at the north east are considered as a unique circular vent (white circle) in this study. The pit at the south-west is considered as a separated vent. (b) The pits are too closed and the pit identified at the north-east by Thomas et al., (2014) cannot be approximated by a circle. The faculae around these pits are not analyzed here.*

Table S1: *Pits displaying a spectral anomaly but not measurable.*

	ID			Crater/Facula Name	Central latitude	Central longitude	Area (km²)	SL
1	K37	J57	5039	Picasso	3,54	50,98	680,97	5
2	-	-	5084	-	-52,85	38,21	154,4	5
3	-	-	5084	-	-52,67	38,64	40,15	5
4	-	-	6096	-	-59,91	145,33	98,92	3
5	-	-	6096	-	-59,39	144,9	5,56	4
6	-	-	6096	-	-59,57	145,04	14,58	5
7	-		6119		-45,78	134,83	42,7	5
8	-	J72	6119	Sher Gil SW	-45,45	134,81	6,8-	5
9	-	J77	6119	Sher Gil SE	-45,51	135,44	86,3	5
10	-	J74	6119	Sher Gil S	-45,15	135,07	17,52	5
11	-	J73	6119	Sher Gil NW	-44,83	134,65	23,78	5
12	-	J76	6119	Sher Gil N	-44,76	134,99	32,32	5
13	-		6125	-	-64,48	144,78	14,21	5
14	-		6125	-	-64,22	143	10,41	5
15	-	J86	6125	-	-64,2	143,59	20,67	5

16	-		6125	-	-63,99	143,49	10,52	5
17	-		6125	-	-63,9	142,66	13,5	5
18	-		6125	-	-64,04	142,07	196,86	5
19	-		6125	-	-63,83	143,08	36,6	5
20	-		6125	-	-63,69	142,59	22,95	5
21	-		6125	-	-63,53	142,57	7,93	5
22	-		6125	-	-63,47	142,13	34,3	5
23	-		6125	-	-63,41	142,74	9,12	5
24	-		6125	-	-63,19	142,6	23,32	5
25	-		6125	-	-63,04	142,49	22,33	5
26	-		6125	-	-62,85	142,49	71,17	5
27	-		6125	-	-62,22	142,07	15,15	5
28	-		6125	-	-62,09	144,34	55,11	5
29	-	J93	6126	-	-65,54	147,64	45,62	4
30	-	J94	6126	-	-65,21	147,76	170,75	4
31	-	-	7019	-	40,44	-100,12	79,1	4
32	-	-	7019	-	41,24	-100,63	468,7	4
33	-	-	7019	-	41,33	-101,81	53,6	3
34	-	-	7019	-	41,03	-102,09	69,8	2
35	K10	J20	7031	To Ngoc Van	52,56	-111,65	323,2	4
36	K26	J26	7057	Unnamed crater 1	21,8	-67,37	195,1	5
37	-	J22	7058	Rumi	-24,12	-105,02	92,5	5
38	-	J11	7090	Tyagaraja	3,8	-148,66	66,2	3
39	-	J6	7107	Tolstoj SE	-19,87	-161,07	26,05	5
40	-		8020		-59,37	-34,41	11,66	4
41	-		8020		-59,16	-33,98	22,7	4
42	-		8020		-59,02	-33,11	38,28	4
43	-		8020		-58,88	-32,59	26,34	4
44	-		8020		-58,76	-32,64	15,13	4
45	-		8020		-57,97	-32,11	119,89	4
46	-		8020		-57,81	-29,42	8,48	4
47	-		8020		-57,86	-29,81	35,05	4
48	-		8020		-57,56	-30,72	22,92	4
49	-		8020		-57,66	-33	59,97	4
50	-	J33	8020	Unnamed crater 6	-57,46	-29,12	79,28	4

Table S2: *Magmatic abundances (ppm) of most probable volatile species required to emplace the measured faculae. The uncertainties related to the uncertainty of the radius (± 5 km) correspond to 1150 ppm CO, 1800 ppm CO_2, 2700 ppm SO_2, 700 ppm H_2O and 1400 ppm H_2S.*

	CO		CO_2		SO_2		H_2O		H_2S	
Crater/Facula Name	**Kerber et al., (2011)**	**This study**	**Kerber et al., (2011)**	**This study**	**Kerber et al., (2011)**	**This study**	**Kerber et al., (2011)**	**This study**	**Kerber et al., (2011)**	**This study**
Mistral SE	4300	6900	6800	11000	9900	16600	2800	4800	5600	8400
Mistral NW	2600	5800	4100	9200	6000	13800	1700	4000	3300	7000
Lermontov NE	7600	10000	12000	16600	17000	24800	4900	7200	9800	12600
Lermontov SW	7200	12700	11000	20200	17000	30400	4700	8900	9300	15400
Praxiteles SW/Orm	4100	6900	6500	11000	9400	16600	2700	4800	5300	8400
Praxiteles NE/Orm	600	6900	9400	11000	14000	16600	3800	4800	7700	8400
Rachmaninoff/Nathair	16000	32200	26000	51500	37000	77300	11000	22500	21000	39300
Caloris/Agwo	5600	10400	8700	16600	13000	24800	3600	7200	7000	12600
Caloris/RS-03 SW	4300	8100	6700	12900	9800	19300	2800	5600	5500	9800
Caloris/RS-04b	4600	5800	7200	9200	10000	13800	3000	4000	5900	7000
Glinka	3800	5800	6000	9200	8700	13800	2400	4000	4900	7000
Enheduanna	3500	8100	5400	12900	7900	19300	2200	5600	4400	9800
Geddes	5000	6900	7800	11000	11000	16600	3200	4800	6400	8400
Hesiod/Pampu	7000	10400	11000	16600	16000	24800	4500	7200	8900	12600
Hesiod/Ular	4500	9200	7000	14700	10000	22100	2900	6400	5700	11200
Hesiod/Sarpa	4900	8100	7700	12900	11000	19300	3100	5600	6300	9800
Hesiod/Havu	2000	4600	3200	7400	4700	11000	1300	3200	2600	5600
Hesiod/Bitin	3200	8100	5000	12900	7400	19300	2100	5600	4200	9800
No name 1	-	6900	-	11000	-	16600	-	4800	-	8400
No name 2	-	10400	-	16600	-	24800	-	7200	-	12600
Neruda	-	9200	-	14700	-	22100	-	6400	-	11200
No name 3	-	13800	-	22100	-	33100	-	9700	-	16800
No name 4	-	4600	-	7400	-	11000	-	3200	-	5600
No name 5	-	5800	-	9200	-	13800	-	4000	-	7000
No name 6	-	10400	-	16600	-	24800	-	7200	-	12600
Unnamed crater 5c	-	6900	-	11000	-	16600	-	4800	-	8400